

GPU-initiated Fine-grained Overlap of Collective Communication with Computation

Kishore Punniyamurthy
Advanced Micro Devices, Inc.
Kishore.Punniyamurthy@amd.com

Bradford M. Beckmann
Advanced Micro Devices, Inc.
Brad.Beckmann@amd.com

Khaled Hamidouche
Advanced Micro Devices, Inc.
Khaled.Hamidouche@amd.com

ABSTRACT

In order to satisfy their ever increasing capacity and compute requirements, many machine learning models are distributed across multiple nodes using space-efficient parallelism strategies. As a result, collective communications are often on the critical path, and hiding their latency by overlapping kernel-granular communication and computation is difficult due to the absence of independent computation.

In this work, we propose fusing computation with communication using GPU-initiated networking, and leverage GPUs’ massive parallelism to enable fine-grained overlap of the fused operations. We have developed a single, self-contained GPU kernel where workgroups (WGs) immediately communicate their results to remote GPUs when they complete their computation. Meanwhile, other WGs within the same kernel perform overlapping computation, maintaining high ALU utilization. Such fine-grain overlapping provides the additional benefit that peak network bandwidth demand is reduced and communication is spread across the entire lifetime of application rather than only at kernel boundaries. Furthermore, we propose zero-copy optimizations for peer-to-peer GPU communication where the data computed by one GPU is directly written to the destination buffers within the peer GPUs, eliminating intermediate stores and extra buffering. Our approach leverages the emerging multi-node GPU system trend where GPUs are physically close to network with direct GPU-NIC interconnects.

We demonstrate our approach by creating an *embedding + All-to-All* fused kernel which overlaps embedding operations and the dependent all-to-all collective in DLRM models. We evaluate our approach both using simulation and real hardware. Our evaluations show that our approach can effectively overlap *All-to-All* communication with embedding computations, subsequently reducing their combined execution time by 31% on average (up to 58%) for inter-node and by 25% (up to 35%) for intra-node configurations. Scale-out simulations indicate that our approach reduces DLRM execution time by $\sim 10\%$ for 128 node system.

1 Introduction

Machine learning is currently being used across wide variety of applications ranging from classification (e.g., fraud detection, medical diagnostics, facial recognition), pattern analysis (e.g., product recommendations, stock price prediction) to content generation (e.g., code generation, chatbots,

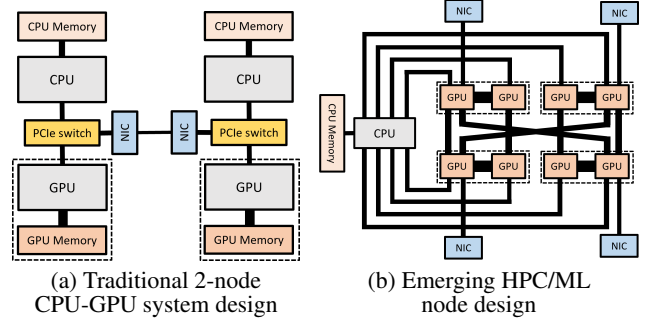


Figure 1: System architecture trends.

image/video generation). Machine learning (ML) models are increasing in size to tackle more complex problems. Studies [52] have shown that the model sizes have increased by 5 orders of magnitude between 2018 to 2022. Large ML models have consequently fueled the development of distributed systems capable of meeting their capacity and compute requirements. Subsequently, parallelization techniques have been developed to efficiently map ML models on to distributed systems [12].

The resulting communication in distributed ML models (e.g., for weight updates, activation exchanges between layers etc.) becomes a significant bottleneck [38, 43] as the system scale grows. Depending on the ML parallelism strategy (e.g., data, tensor, or model parallelism), there may be opportunities to hide or overlap communication with independent compute. For example in data parallel models, *AllReduce* collectives can be overlapped with an independent gradient computation [51, 56]. However, growing model sizes has increased the preference for space-efficient parallelism strategies [47], like tensor-parallelism and fully-sharded data parallelism [8]. Such parallelism strategies often result in collective communication which are difficult to hide due to the absence of independent computation.

ML trends are also influencing system design and architecture development. Figure 1 compares a traditional CPU-GPU multi-node system with a state-of-the-art node design optimized for HPC/ML. Other than compute and memory improvements, we notice two broad trends. Firstly, intra- and inter-node communication bandwidth and latency have been improved using proprietary interconnects [3, 17] and high-bandwidth network interface cards (NICs). Secondly, given the increased preference to use GPUs for ML workloads,

GPUs are becoming the primary computation engine tightly integrated with on-node CPUs and NICs. In addition more and more GPUs are directly communicating with the network using high-radix switches [15] or direct-attached NICs [1, 25]. However, applications have yet to fully embrace these trends and often rely on the CPU [31, 42] to perform remote communication. Recent GPUDirect RDMA [5, 9] technology somewhat combats this and enables data to be directly moved between GPU memory and NIC, but the communication is still triggered by the host CPU and often at kernel boundaries. Such approaches are mostly suitable for bulk-synchronous applications where communication can be overlapped with independent computation at the kernel granularity and the kernel-launch overhead is amortized using large kernels. Using GPUDirect, applications with dependent communication and computation must be tiled and pipelined at the kernel granularity to achieve overlapping. Tiling (with smaller sizes) increases the number of kernel invocations resulting in kernel-launch overhead, while kernel-level pipelining adds GPU stream management overhead. Furthermore, kernel-granular overlap may result in additional computational overhead to merge the individual partial results [53].

In this paper, we aim to address the growing bottleneck of collective communication by fusing and overlapping communication and dependent computation using intra-kernel GPU-initiated networking. Our approach is easy to apply and leverages the existing workgroup-level work partitioning in GPU applications. By immediately scheduling non-blocking network transactions, data fragments are communicated as they are computed without waiting for kernel completion. We have developed a single, self-contained persistent GPU kernel [41] where one or more logical workgroups (WGs) upon completing their share of computations, issue non-blocking transactions to communicate their results to remote GPUs. We demonstrate our approach by creating a fused communication-computation kernel, which is unique compared to existing approaches [26, 27] that exclusively fuse only computation kernels. Specifically we create an *embedding + All-to-All* operator as a persistent kernel which overlaps embedding operations and their dependent All-to-All collective in deep learning recommendation models (DLRM) [44]. We further propose remote communication-aware scheduling of the logical WGs within each persistent WG, where the logical WGs outputting data for remote communication are scheduled ahead of the logical WGs outputting data for local consumption in order to maximize communication overlap. For the locally communicated data, we develop zero-copy fused kernels where the GPU threads directly store their computed results to all-to-all destination buffers.

Unlike prior kernel-granular approaches, our approach overlaps dependent remote communication with computation at the finer granularity of a WG cluster. GPU-initiated communication eliminates the need for CPU resources to perform remote communication and reduces the peak bandwidth requirement because network transactions are spread across the application’s entire execution time. Within peer-to-peer connected GPUs, zero-copy fused kernels eliminate intermediate stores to local GPU memory. Furthermore, our GPU-centric approach embraces the emerging trend of tight GPU-network integration [1, 15] as shown in Fig. 1b.

This paper makes the following key contributions:

- We propose a novel approach to overlap collective communication with computation at a slice granularity using GPU-initiated communication. We propose fused computation-communication kernels that combine collective communication with computation within the same kernel, thus reducing peak bandwidth and CPU resource requirements. Further, we propose zero-copy fused kernels where the results are directly written to the peer GPU memory thereby eliminating intermediate buffering and copy operations.
- We further propose a remote communication-aware WG scheduling optimization where the WGs computing remote embedding slices are scheduled first thereby maximizing the opportunity to overlap remote communication.
- We implement the fused *embedding + All-to-All* operator as a persistent kernel in HIP [10], along with remote communication-aware WG scheduling, and evaluate its benefits using both GPU hardware and simulations. Our evaluations show our approach achieves 31% lower latency than the baseline’s embedding operations and All-to-All collectives.
- We evaluate the design trade-offs for using GPU-initiated communication and highlight the factors critical to achieve effective overlap with low overhead.

2 Background

In this section, we first illustrate the communication bottleneck observed in modern day distributed ML models. We then elaborate on the All-to-All communication bottleneck in DLRM as we use it to demonstrate the effectiveness of our approach. Finally, we provide a background on GPU-initiated communication.

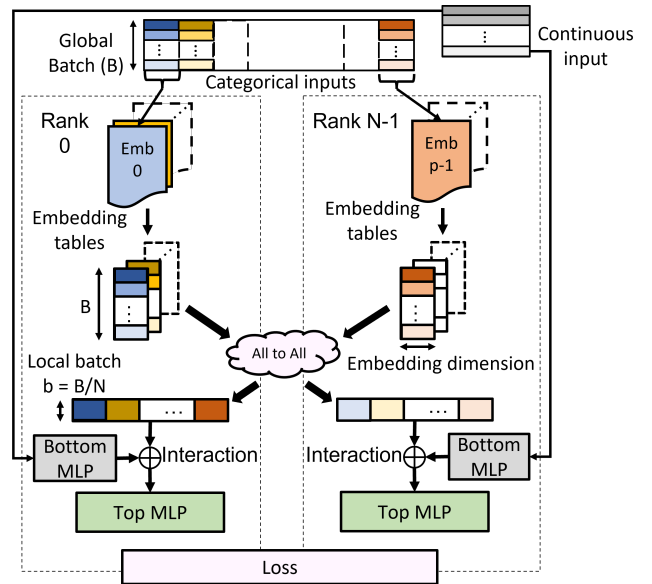


Figure 2: DLRM forward pass.

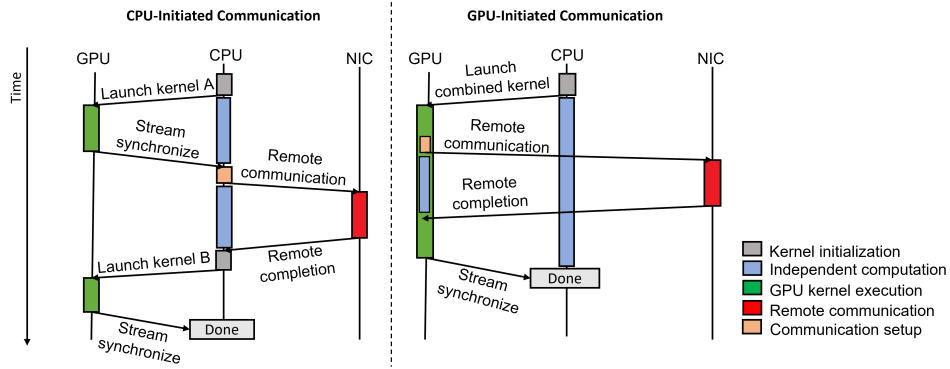


Figure 3: System-level transactions in CPU-initiated vs GPU-initiated communication

2.1 Collectives in Distributed ML Models

As mentioned earlier, modern ML models need to be distributed across a large number of nodes to accommodate their capacity and compute requirements. Due to their large capacity requirements, space-efficient parallelism strategies distribute weights across GPUs avoiding data duplication (e.g., tensor parallelism, fully-sharded data parallelism [8]). However, such strategies result in additional collective communication to train and execute the models. Fully-sharded [8] data parallelism results in *AllGather* collectives to gather the weight matrix from all nodes before performing matrix-matrix multiplication. Mixture-of-experts (MoE) models [38, 46] employ expert parallelism and expert slicing to scale across nodes, resulting in *AllGather* and *All-to-All* collectives in their critical path.

DLRMs are another class of popular models which suffer from the collective communication bottleneck. Due to the large memory requirements of embedding tables, DLRMs typically employ model parallelism for distributing embedding tables across GPUs [44]. Recent works have proposed using table, row, and column parallelism [43] depending on the size and count of the tables (data parallelism can be potentially used for small tables). The top multi layer perceptron (MLP) layers of DLRM use data parallelism for scaling across multiple GPUs. In order to switch from model parallelism execution (for embedding operations) to data parallelism (for top MLP layers), *All-to-All* collective operations are used [44] as shown in Figure 2.

The operations/layers involved in DLRM models (embedding vector pooling, *All-to-All*, top and bottom MLP) are executed in bulk-synchronous manner which prevent communication from being overlapped with dependent computation. From the above Figure 2, we can see that bottom MLP layers are the only independent kernel-level computation available to be overlapped with the *All-to-All* collective. However, bottom MLP layers are usually small and thus cannot hide *All-to-All* communication effectively. Prior research has shown that *All-to-All* latency is exposed (>35% of execution time) and has direct impact on overall latency in state-of-the-art systems [43].

2.2 GPU-initiated RDMA networking

Remote Direct Memory Access (RDMA) technology bypasses the target CPU when performing inter-process network communication and is implemented in many high-performance networking protocols [11, 22]. RDMA communication is usually performed by the host CPUs (e.g., MPI [13], OpenSHMEM [20] and RCCL [23]) and such CPU-initiated RDMA networking is widely used for distributed computing in HPC workloads [31, 42]. GPU-based HPC and ML systems typically use GPUDirect RDMA [9] and associated programming models (e.g., CUDA-Aware MPI [5]) to enable direct data transfers between GPU and NIC, bypassing the CPU memory. Such approaches provide better latency than vanilla CPU-initiated communication and are widely used in GPU-based HPC [35, 39] and ML applications [14, 23]. While GPUDirect based communication eliminates unnecessary data copies to/from CPU memory, it still requires host CPU to trigger the network transactions resulting in transfer of control between CPU and GPU.

The recent trends of direct GPU-to-GPU [15] and GPU-to-NIC [25] integration in HPC and ML system design have created an opportunity for GPU-initiated RDMA networking and corresponding programming models. This technology allows GPU threads to directly communicate with NICs using command queues, thereby bypassing the host CPUs. Vendor-specific GPU libraries (e.g., NVSHMEM [18], ROC_SHMEM [24]) have been developed that enable applications to perform intra-kernel GPU-initiated communication while adhering to a partitioned global address space (*OpenSHMEM* [20]) programming model. Moreover, recent GPU micro-architecture features are facilitating GPU-initiated networking further. For example, prior versions of ROC_SHMEM required data to be allocated as un-cacheable in order to prevent stale data from being communicated to remote nodes. However, the recent introduction of intra-kernel cache flush instructions [4] allow GPU threads to flush the data before initiating network transactions, thus allowing data to be cached during computation. Further, new programming abstractions such as threadblock cluster [16] can enable faster coordination between WGs to perform intra-kernel network communication.

Figure 3 compares and contrasts the system interactions

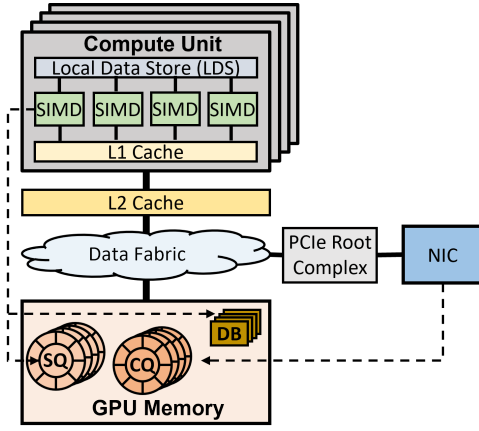


Figure 4: GPU-initiated communication design [36]

on using CPU-initiated vs GPU-initiated communication. In CPU-initiated communication, kernel performing the computation has to complete before the remote/network communication can be triggered. Further, the control is passed to CPU which then issues the remote communication. On completion of the remote communication, CPU then launches the kernel to perform dependent computation. The transfer of control from GPU to CPU and back adds overhead to the application execution time and consumes CPU resources which could have been used for other computations [57]. Additionally, techniques like double-buffering and GPU streams will have to be used to ensure high GPU utilization. In the absence of independent work, applications will have to be broken into smaller independent kernels where each smaller kernel is executed as a separate stream and computation of one stream is overlapped with the communication of a different stream. This approach can result in large number of small kernels and add significant kernel launch and stream management overhead [40, 43, 55].

GPU-initiated communication allows GPU threads to directly issue remote communication commands to the NIC eliminating the need to transfer control to CPU. Further, there is no need to split the kernel. Instead GPU-initiated communication allows GPU threads to issue remote communication while others are performing computation enabling fine-grained communication and computation overlap.

Figure 4 shows the underlying design of GPU-initiated communication used in ROC_SHMEM [24, 36]. The *Send Queue (SQ)* and *Receive Queue (RQ)* are where the GPU threads post command packets for the NIC to execute, and the *Completion Queue (CQ)* is where the NIC posts the status of a completed operation. These structures are often collectively referred to as a *Queue-Pair (QP)*. These queues are allocated in GPU memory to facilitate low-latency access by GPU threads. For initiating a remote communication, GPU threads first create a network packet within the SQ. The packet contains information such as source, destination address, destination node, operation type. GPU thread(s) then ring the NIC doorbell (DB) which are I/O mapped NIC registers. The NIC then processes the individual packets and performs the corresponding communication. GPU threads can wait on the completion packet which is posted by NIC

into the CQ to determine the completion of the remote communication.

3 Fused Computation and Communication

In this section, we first explore the opportunity for overlapping fine-grain embedding computations in DLRM models with dependent All-to-All communication. We then discuss the design and implementation of our fused *embedding + All-to-All* operator and its integration within the DLRM computation graph. Finally, we describe our zero-copy fused kernel that optimizes peer-to-peer GPU communication before discussing the overheads associated with our approach.

3.1 Fine-grained Overlapping Opportunity

In order to achieve fine-grained overlapping of dependent computation and communication, we leverage WG-granular compute partitioning prevalent in GPGPU applications. In DLRM [7], for every categorical input, the embedding operator (*EmbeddingBag_updateOutputKernel_sum_mean*) accesses one or more vectors from the embedding table and pools (reduction-like operation) them to generate the corresponding output vector. This pooling operation is parallelized such that 64 (=wavefront size) embedding vector elements are pooled by each wavefront. If we assume the size of each embedding vector (embedding dimension) to be 256 elements, and WG to be 256 threads large, each WG will compute one output entry independent of other WGs. As the WGs performing embedding pooling finish computing their respective output fragment, they can issue a non-blocking remote communication to move their generated output. The non-blocking nature of this communication and the concurrently computing WGs on the same CUs allow us to achieve high compute utilization while hiding communication.

While intra-kernel, WG-granular communication provides programmers a natural way to hide communication latency, the resulting packet sizes can be too small to be efficiently

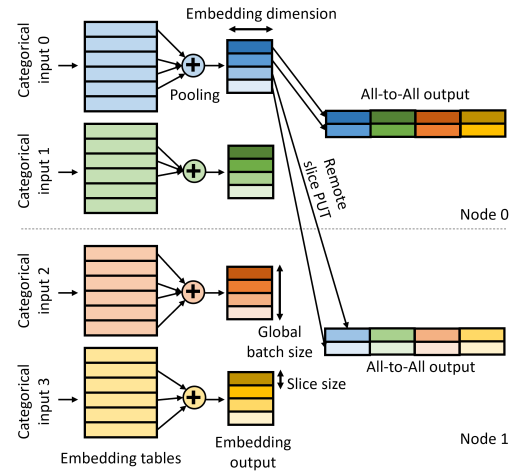


Figure 5: Fine-grained overlapping of embedding operations with communication.

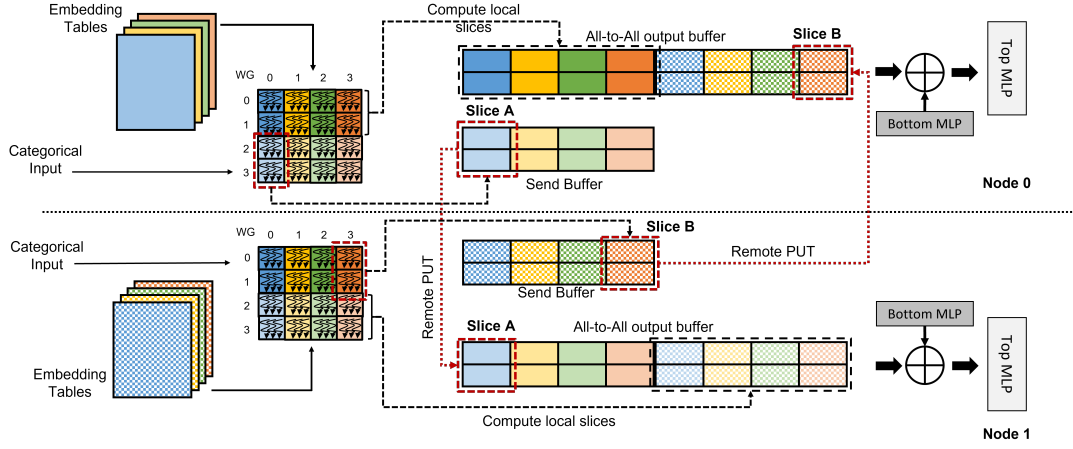


Figure 6: Embedding + All-to-All fused operator

transmitted over the network. We mitigate this by performing remote communication once a *slice* (slice size is a parameter) of output data is computed by a cluster of WGs. Figure 5 shows All-to-All collectives being executed using WG-triggered point-to-point network *Send/PUT* operations with embedding dimension sized slices. Since each slice is independent and is computed by a separate cluster of WGs, a slice can be communicated while others are being computed.

3.2 Fused Embedding + All-to-All Operator

In this work, we develop a single persistent GPU kernel in HIP [10] which performs both embedding computations and All-to-All communication. We use ROC_SHMEM [24] GPU APIs to issue network communication from within the device kernel. The proposed fused kernel eliminates the need to transfer control to CPUs for collective communication and reduces peak bandwidth requirement as the network requests are spread over application’s lifetime. Furthermore, since our fused operator is implemented as a single, self-contained GPU kernel, our approach results in fewer kernel invocations, and lower CPU and GPU hardware resource usage (e.g., *hipStream/cudaStreams* and CPU threads to manage the execution streams).

Figure 6 shows an example execution of our proposed fused operator. It illustrates a two node system where embedding tables are distributed in model parallel fashion such that there are four tables per node. We implemented our fused *embedding + All-to-All* operator as a persistent thread (PT) kernel [33, 41] which performs embedding pooling for all tables allocated within the node. This allows us to schedule logical WGs computing the same slice together (similar to the approach used in [41]) and further reduces the number of kernel invocations. The kernel is launched with a fixed, input-independent grid size (less than or equal to maximum occupancy as determined from the HIP occupancy API [19]). Each persistent WG executes a task loop where every iteration corresponds to the computation performed by a logical WG of the original embedding kernel (*Embedding-Bag_updateOutputKernel_sum_mean*).

The tables and WGs shown in Figure 6 are color coded

to indicate WGs and the tables they are processing. Note that the WGs shown here represent the logical WGs and not the persistent WGs. Our fused kernel takes in categorical inputs and embedding tables as kernel arguments. In this example, we assume the global batch size to be four, the slice size to be two embedding output vectors, and that each output embedding vector is computed by one WG. Since there are two nodes, the pooled output embedding vectors from each table are shuffled equally across both the nodes (two output vectors each), with first half of global batch stored in node 0 and second half in node 1. Depending on their embedding slice, the WGs may need to store their results locally or communicate them to the remote node. The index of the slice computed by a WG can be determined using the output embedding entry computed and size of the slice. The slice index along with the global batch size and node count can then be used to determine if the slice needs to be communicated remotely. Logical WGs *WG 00 - WG 13* compute the output corresponding to the first half of global batch, while *WG 20 - WG 33* compute the latter half. For node 0, *WG 00 - WG 13* compute the output entries consumed locally, while results of *WG 20 - WG 33* will have to be communicated to node 1. While for node 1, results from *WG 00 - WG 13* are communicated to node 0 and *WG 20 - WG 33* store their results locally.

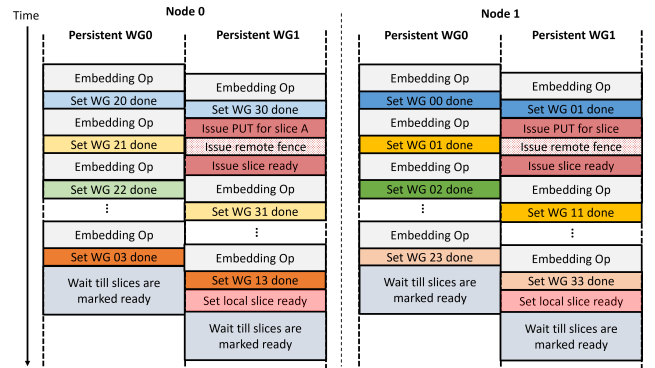


Figure 7: Execution timeline of persistent WGs.

As described earlier, our approach performs communication at a granularity of a *slice*. The size of each slice is set to match the output computed by one or more WGs (user parameter). In the example shown in Figure 6, a slice is equal to two output embedding vectors and is computed by two WGs. For example, *WG 20* and *WG 30* compute slice A on node 0. While there can be multiple WGs responsible for computing a single slice, the remote communication to move the slice is initiated by the last WG that finishes the corresponding slice. In the example shown, assume *WG 30* finished its computation for slice A after *WG 20* (e.g., due to wavefront scheduling effects). Then, a thread from *WG 30* will issue the remote communication (Remote PUT) to move slice A to node 1. We track the completion of logical WGs corresponding to every slice to identify the last completing WG and trigger communication accordingly. Implementing All-to-All using point-to-point transactions allows the communicating WGs to move the slice data to the destination in a layout required by any subsequent kernel (e.g., the interaction operation in DLRM). The output data can be shuffled at a slice granularity without requiring explicit shuffling or rearrangement. In our approach, we generate output with the shape: {local batch size, (numTables \times embedding dimension)}, which can then be passed to the *interaction* operator.

In our approach, we maintain two sets of flags (not shown in Figure 6) per GPU to synchronize WG communication and determine the end of communication. First, we maintain a *WG_Done* bitmask per slice where each bit indicates the completion status of the logical WGs (iteration in task loop). This bitmask is used to identify the last finishing WG and issue remote communication. Second, we maintain a *sliceRdy* flag per slice (both locally computed and received remotely) to indicate if all the individual slices have been received (or computed) and are ready for consumption by subsequent kernels.

Figure 7 shows the execution timeline of the persistent WGs for the example illustrated previously. Assume there are two persistent WGs per node, each performing the work of 16 logical WGs iteratively. We propose and implement remote communication-aware logical WG scheduling within the persistent WGs. In our approach, logical WGs computing slices for remote communication are computed ahead of WGs computing locally consumed slices, thereby maximizing the opportunity to overlap remote communication. For example, persistent WGs in node 0 compute *WG 20* and *WG 30* before computing *WG 00* and *WG 10* so that the remote communication can be overlapped with computation of local slices. Upon completion of each logical WG (an iteration within the task loop), a leader thread sets the bit corresponding to the logical WG in the *WG_Done* bitmask as shown in the timeline. The WG also checks if it is the last one to complete by testing if all the other bits in the bitmask are set. This design allows the WGs to make forward progress after setting their respective *WG_Done* flag instead of waiting on an inter-WG barrier. The last completing WG issues two remote PUT calls separated by a remote fence. The first call is to move the slice data, while the second sets its corresponding *sliceRdy* flag on the remote node to indicate that the slice has been copied. The remote fence ensures that the *sliceRdy* flag is only set after the prior PUT has completed. After executing all the

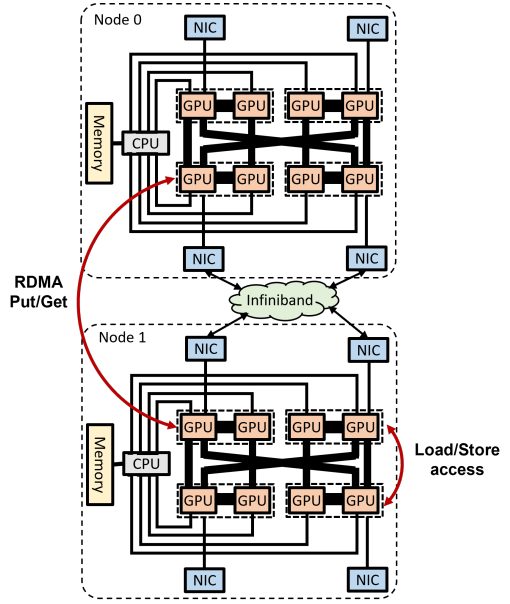


Figure 8: Inter-node vs P2P communication

logical WGs, the persistent WGs poll on a distinct subset of *sliceRdy* flags before exiting. This ensures that the data from all slices are ready for subsequent kernels while incurring less overhead than having all WGs poll on the entire set of *sliceRdy* flags.

Our current implementation overlaps communication with computation at WG cluster granularity (one or more WGs) but the same idea can be extended to thread- or wavefront-granularity.

3.3 Zero-copy Fused Communication

Figure 8 shows a two node system where GPUs are connected peer-to-peer (P2P) within the same node (interconnected using xGMI [3], or NVLink [17]) and use infiniband to communicate with GPUs across nodes. Unlike remote GPUs which require RDMA network transactions (enabled using ROC_SHMEM API calls) to communicate, P2P GPUs can communicate using native GPU load/store instructions. We exploit this feature to further optimize our fused kernel for P2P GPUs. Existing collective libraries [23] use GPU threads to perform P2P communication. However, due to bulk-synchronous execution, the embedding outputs are first stored into an intermediate buffer within local GPU memory before being communicated to the peer GPUs using a dedicated copy kernel. We create zero-copy fused kernel, where in-addition to overlapping dependent communication and computation, we eliminate the stores to intermediate buffers by directly writing the output to the peer GPU memory. As the embedding vectors are pooled, GPU threads directly store the output to the destination address, if located within a peer GPU. We use *roc_shmem_ptr()* API [24] to determine if the target GPU is a peer. The call also returns the virtual address corresponding to the destination memory buffer within the peer GPU, to which the stores can be performed. This abstraction allows inter-process communication between P2P GPUs,

and achieves code portability across systems with different intra-node and inter-node configurations.

We demonstrate zero-copy fused kernels on a single node, multi-GPU configuration. However, this approach is even more effective for systems where P2P communication can be performed across a large number of GPUs [15].

3.4 Overheads

While GPU-initiated networking eliminates the use of CPU resources for communication and enables fine-grained dependent communication-computation overlap, it consumes GPU resources which can impact performance.

API latency: An obvious overhead of having GPU threads issue networking transactions is the latency overhead of the APIs. The impact of this overhead is limited as the communication is only triggered once per slice. However, there are other book-keeping operations which need to be performed which adds additional overhead. Every WG has to set its corresponding *WG_Done* flag in order to synchronize communication. Further, additional logic must determine the logical WG identifiers executed by the persistent WGs in accordance with the communication-aware scheduling.

Occupancy: ROC_SHMEM [36] uses *local data store* [1] (LDS) to store WG communication contexts for faster access, reducing the amount of available LDS for the application and subsequently limiting kernel occupancy. Similarly, invoking ROC_SHMEM API calls consume GPU registers which otherwise would have been used by the application. Reduced register availability can result in lower occupancy or increased register spilling, impacting performance. Embedding operations do not use any LDS, so LDS usage does not impact its occupancy, but reduced register availability causes our fused kernel implementation to achieve 12.5% lower occupancy compared to original embedding pooling (*EmbeddingBag_updateOutputKernel_sum_mean*) kernel. Despite lower occupancy, our approach achieves better performance as shown in Section 4.

Inter-WG synchronization: In our approach, communication is triggered once for every slice of data. Since multiple WGs could be computing an individual slice, inter-WG synchronization is required. Our implementation does not use inter-WG barrier and instead cross-lane operations [2] reduce the *WG_Done* bitmask to ensure only the last completing WGs issue the remote communication.

Software integration: Existing GPU-initiated networking libraries [18, 24] use OpenSHMEM [20] programming model and subsequently require a symmetric heap to be allocated across all participating GPUs. The source and destination buffers used for GPU-initiated communication must be allocated within the symmetric heap. Allocating buffers within this heap requires a library-specific memory allocator (e.g., *roc_shmem_malloc()* for ROC_SHMEM). Integrating GPU-initiated networking within existing ML frameworks will require custom memory allocators [6] to allocate tensors on symmetric memory. Note that the benefits of GPU-initiated networking are not dependent on OpenSHMEM semantics and the libraries can be extended to use existing GPU mem-

Table 1: Hardware setup.

GPU	AMD Instinct™ MI210
Software	Pytorch v1.12, ROCm v5.2, ROC_SHMEM v1.5
Intra-node	
# GPUs	4 (fully connected)
Interconnect	xGMI links, 80GB/s
Inter node	
# Nodes	2 (each with x1 GPU)
Network	Infiniband, 20 GB/s

Table 2: Scale-out evaluation setup.

Model Parameters [43]	
Embedding dimension	92
Avg. MLP size	682
Num MLP layers	43
Avg. pooling size	70
ASTRA-Sim Network Parameters [49]	
Topology	2D Torus
Bandwidth	200 Gb/s
Latency	700 ns

ory allocators. The tensors can then be registered with NICs using dedicated API calls.

3.5 General Applicability for Collectives

In this work, we focus on the *embedding + All-to-All* fused operator to demonstrate the use of GPU-initiated networking for overlapping dependent communication and computation. However, benefits of overlapping dependent computation with communication are not restricted to this. For recommendation models which are MLP heavy [34], *All-to-All* can be overlapped with one or more matrix multiplication operations. In fully-sharded [8] data parallel models, the *AllGather* collective can be overlapped with the subsequent matrix computations. Similarly, *AllGather* and *All-to-All* collectives in MoE models [46] can be overlapped with subsequent computation by creating their corresponding *AllGather* + computation, and *All-to-All* + computation fused kernels using GPU-initiated communication.

4 Evaluation

We implemented our fused *Embedding + All-to-All* kernel using HIP and evaluated it both using simulation and on actual hardware. For real hardware, we used both 4-GPU intra-node and 2-GPU inter-node configurations, and for simulation we used a 128-node scale-out configuration.

4.1 Setup

We compared our fused operator implementation against the embedding operations (embedding dimension=256 [43]) and

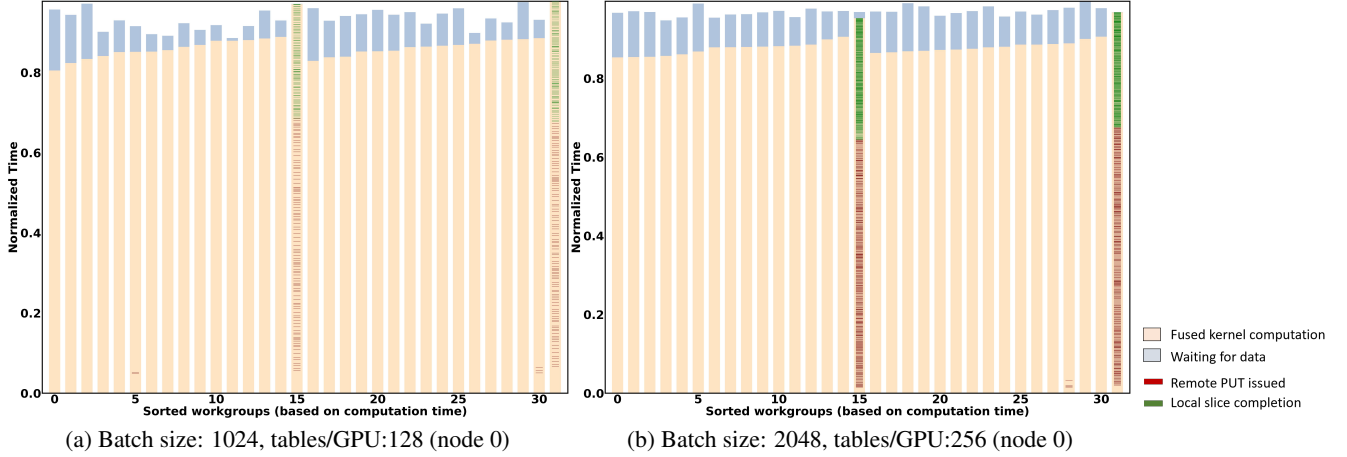


Figure 9: Profiled timeline of persistent WG.

All-to-All collectives implemented in the publicly available DLRM [7] code. The baseline DLRM uses RCCL [23] to perform All-to-All collectives and Table 1 shows the system setup used for our evaluations. We varied the global batch-size and the number of embedding tables processed per GPU across different inter-node and intra-node configurations. Each configuration is labeled as: $\langle \text{global batch size} \rangle | \langle \text{embedding tables per GPU} \rangle$ in the graphs (unless stated otherwise). For inputs, we used the data generator in DLRM.

For the scale-out configuration, we evaluated the entire DLRM [7] application in ASTRA-Sim [48]. We modified ASTRA-Sim’s execution graph to model our fused *embedding* + *All-to-All* kernel. The DLRM model and simulator parameters used are shown in Table 2. The per-kernel execution times used in ASTRA-Sim were collected on an AMD Instinct™ MI210 GPU using ROC-profiler [21].

4.2 Inter-node evaluation

WG Profiling: We first demonstrate the effectiveness of overlapping embedding operations with All-to-All communication. We profile the persistent WGs’ execution timelines for two different configurations and the slice size is set such that each slice is computed by 16 WGs. WGs computing the same slice (cluster of 16) are sorted based on their time to complete embedding pooling operations (earliest first). Figure 9 illustrates the execution timelines for the first 32 persistent WGs along with the points in time when non-blocking network transactions were issued. Figure 9 also shows the points in time when locally consumed slices are computed (marked as *Local slice completion*) to illustrate the effect of communication-aware scheduling. One key observation to note is that some persistent WGs are issuing remote communication, while others are performing the computation, demonstrating our approach achieves fine-grained communication-computation overlap. Further, non-blocking network transactions allow the communicating WGs (e.g., WG 15 and 31) to continue performing embedding pooling without being blocked.

Figure 9 shows that the last WGs (WG 15 and WG 31)

within each cluster of 16 WGs issues most of the communication. The main reason behind this is each persistent WG computes the individual slices iteratively. The last completing WG for one slice often stays the last across multiple slices (please recall that only the last completing WG issues the remote non-blocking PUT call). Additionally, from the timelines we can see that the remote communication calls are issued before computing the local slices, maximizing the opportunity to hide remote communication. The amount of time spent waiting on data differs across WGs because each persistent WG waits for a distinct subset of data.

Execution time: Figure 10 shows the time taken by our fused embedding + All-to-All kernel normalized to the baseline performing separate kernel-granular embedding operations and All-to-All collectives. Our fused kernel uses a slice size of 32 embeddings. Overall, Figure 10 demonstrates that our approach provides benefit across a wide set of batch sizes and embedding table counts, achieving 31% reduction in execution time on average (and up to 58%). For smaller global batch sizes (e.g., 256), we note that the performance benefit is more than what could be achieved by fully overlapping communication. This is because smaller batch sizes result in poor compute utilization for the baseline, while our approach achieves much higher compute utilization by processing all embedding tables within a single fused kernel.

Occupancy effect: Our fused kernel implementation results in 12.5% lower GPU occupancy than the baseline due to the extra registers required by GPU-initiated networking operations. However, this loss of occupancy does not degrade performance. Figure 11 shows the variation in the execution time of the fused embedding + All-to-All kernel (global batch size: 1024, tables/GPU: 256) under different kernel occupancy. We only show results up to 87.5% occupancy because that was the maximum our implementation could achieve relative to baseline. We see that as the occupancy is increased from 25% to 75%, the parallelism increases and consequently the execution time reduces by 46%. However, increasing the occupancy further from 75% to 87.5% results in the execution time increasing by 25%. At this higher

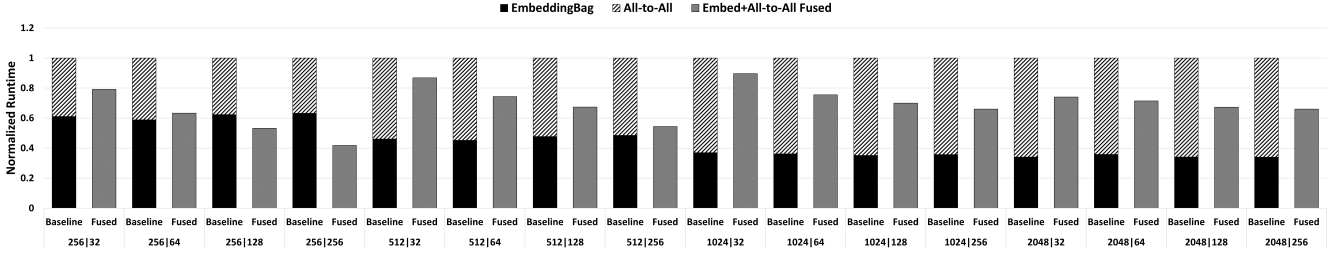


Figure 10: Normalized execution time (inter-node).

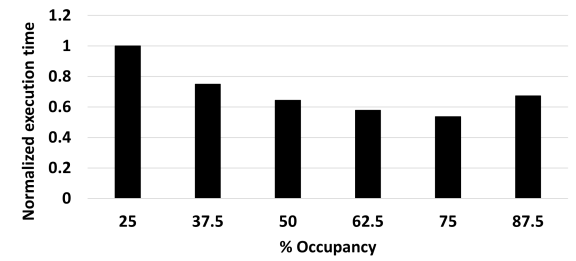


Figure 11: Impact of WG occupancy on execution time.

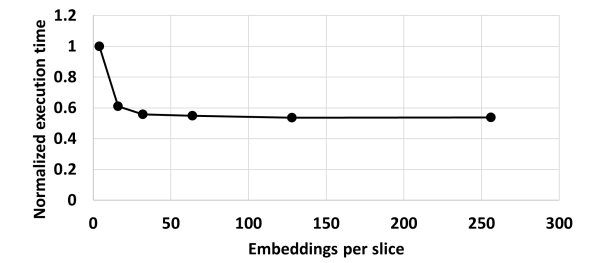


Figure 12: Impact of slice size on execution time.

occupancy level, the memory intensive embedding operations encounter significant memory contention, exemplifying the trade-off between parallelism achieved and memory contention. The optimal number of concurrent WGs will vary depending on batch size and table count.

Sensitivity to slice size: Our approach uses size of each slice as a parameter to determine the granularity of overlap and the amount of data transferred per network transaction. Smaller slices will result in finer computation-communication overlap but the resulting data transfer cannot effectively utilize network bandwidth. Further, smaller slices will require the NICs to process higher number of messages, creating a message rate-bound bottleneck. Figure 12 shows the variation in normalized execution time of fused embedding + All-to-All kernel (global batch size: 1024, tables/GPU: 256) as the size of each slice is increased. We can see that the execution time reduces as the slice size is increased and then saturates beyond 64 embeddings per slice. Configuration with a slice = 64 embeddings has 16x larger messages and results in 16x fewer number of messages compared to a configuration with slice size of four embeddings, subsequently the former achieves $\sim 55\%$ lower execution time than the latter.

Communication-aware Scheduling: In our approach, we implement communication-aware WG scheduling to maximize the opportunity to hide remote communication. Figure 13 shows the fused *embedding* + *All-to-All* kernel execution time of both nodes (normalized to baseline: node 0) with and without communication-aware scheduling. The baseline communication oblivious scheduling starts from WG (0,0,0) and then proceeds sequentially. We can see that in baseline, node 0 and node 1 have an average skew of $\sim 7\%$ in their execution time while using communication-aware scheduling exhibits only a $\sim 1\%$ average execution time skew. Many dis-

tributed ML models including DLRM periodically synchronize across nodes (e.g., during synchronous gradient descent), and thus execution skew can subsequently reduce the overall system performance. The high skew in baseline is due to the higher execution time for node 1. As part of our fused kernel implementation, WGs in node 1 will wait for slices from node 0 and vice-versa. Node 1 has the same logical WG schedule under both strategies, where it first computes the slices to be communicated to node 0 (please see Figure 7). However, with the baseline communication-oblivious scheduling, node 0 computes the slices to be remotely communicated after the locally consumed slices. Thus the remote communication is not hidden behind local slice computation, delaying the completion of node 1.

4.3 Intra-node evaluation

We evaluated the benefits of zero-copy, fused kernel on a single node with four GPUs inter-connected using xGMI links. As part of our zero-copy fused kernel each GPU thread directly stores the computed result at the destination address. Since only P2P GPUs are involved in this case, all the communication is performed at GPU thread granularity (not slice) using P2P GPU stores. Thus, there is no need to launch the kernel in a persistent manner. For this configuration, we launch a zero-copy fused kernel per table similar to the baseline. Figure 14 shows the execution time of our approach normalized against time taken for embedding operations and intra-node All-to-All. Overall, our approach achieves on average 25% (and up to 35%) lower execution time. The benefits achieved are lower for smaller batch sizes (e.g., 512) due to the small All-to-All latency. While for larger batches we observe higher benefits than what could be achieved by fully overlapping All-to-All. This additional benefit is due to the zero-copy optimizations which eliminate stores to intermedi-

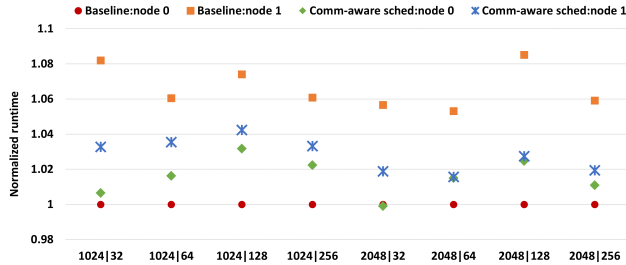


Figure 13: Impact of communication-aware WG scheduling.

ate local buffer.

4.4 Scale-out evaluation

We evaluated the benefits of our approach on DLRM training distributed across 128 nodes (with one GPU each) using ASTRA-Sim. Figure 15 shows the normalized execution time for performing one DLRM training pass for our approach normalized against the baseline. The embedding operations and All-to-All collective communication involved in the forward pass of DLRM is replaced with our proposed fused *embedding + All-to-All* kernel. The extent of the benefit which can be achieved from our approach is limited by minimum of the overlapping operations. We can see that our approach is able to hide most of embedding operations behind All-to-All, achieving on average $\sim 10\%$ reduction in the overall execution time. Note that, the benefits currently achieved are by overlapping the All-to-All involved in the forward pass. Fusing the All-to-All collective with dependent computation along the backward pass will provide additional speed-up.

5 Related Work

To the best of our knowledge no prior work has addressed hiding All-to-All latency in DLRM using GPU-initiated communication. However, there have been prior research on optimizing DLRM, overlapping communication-computation using CPU-initiated networking, GPU-initiated communication for ML, and optimizing collective communication which we present in this section.

Ever since the DLRM models were released [7], researchers have been proposing techniques to improve their execution performance and memory-efficiency. Mudigere et al. [43] proposed Neo system which employs 4D parallelism strategy (table-wise, row-wise, column-wise, and data parallelism) for distributing embedding computations evenly across GPUs. Furthermore, they fuse embedding operators with their parameter update into single kernels to minimize kernel-launch overheads and memory requirements and employ software-managed caching mechanism to leverage hardware memory hierarchy. Their evaluations show that All-to-All latency is exposed and constitutes a significant portion ($>35\%$) of distributed DLRM training execution time. Other research works have proposed ways to reduce memory consumed by embedding tables using compression [32, 50] and improving data layout by leveraging the asymmetrical access patterns of embedding tables [28]. However, in this paper, we try to

address large All-to-All communication latency exposed in distributed DLRM training. We do so by fusing and overlapping All-to-All with embedding operations at finer granularity using GPU-initiated communication.

Wang et. al [53] propose decomposing the original collective communication and its dependent computation into smaller pieces. The communication of an individual data shard can be overlapped with the computation of another. Our approach is conceptually similar to this as both aim at overlapping communication of a portion of data with the computation of another. However, unlike us, the approach proposed in [53] will result in higher number of kernel invocations where each sharded kernel is smaller than the original one. For the use case considered in [53], the sharded kernels (corresponding to individual data shard) are sufficiently large to amortize the kernel invocation overhead but this is not always the case [43]. Further, their approach uses CPU resources to manage and schedule the sharded kernels and requires additional operations to combine the individual partial results. Our approach uses GPU-initiated networking to eliminate CPU resources for communication and leverages the application compute distribution across WGs to hide communication without requiring additional computation to merge results.

Wang et. al. [54] propose using GPU-initiated networking to hide remote memory access latency in GNNs. While this work uses GPU-initiated communication, it focuses on optimizing irregular communication by interleaving and pipelining local neighbor aggregation with remote neighbour access. Their work targets a different problem than that addressed in this paper and thus require completely different optimizations and implementation.

Unlike our approach which aims at hiding the collective communication latency. There have been efforts to reduce the collective latency. Cai et. al. [30] have proposed an approach to synthesize collective algorithms tailored for a specific hardware topology. Others [37, 49] have proposed optimal communication schedule for specific collectives aimed at reducing contention and improving link utilization. These optimizations are orthogonal to the approach proposed in this work.

Fusing kernels/layers/operators into a single operator to eliminate intermediate stores has been proposed in the past [29, 45] and is widely prevalent in modern ML frameworks [26, 27]. However, in existing approaches the kernels being fused together are exclusively compute operations. We instead propose fusing communication with computation as part of our approach.

6 Conclusion and Future Work

The capacity and compute requirements of large ML models have necessitated the need to distribute the models across multiple nodes. Many of the popular parallelism strategies used for such large ML models result in collective communications (e.g., *All-to-All*, *AllGather*) as part of their training and execution. Such collectives are difficult to overlap with computation due to their dependencies, and thus their latency is exposed as part of the total execution time. This collective communication is quickly becoming a significant bottleneck

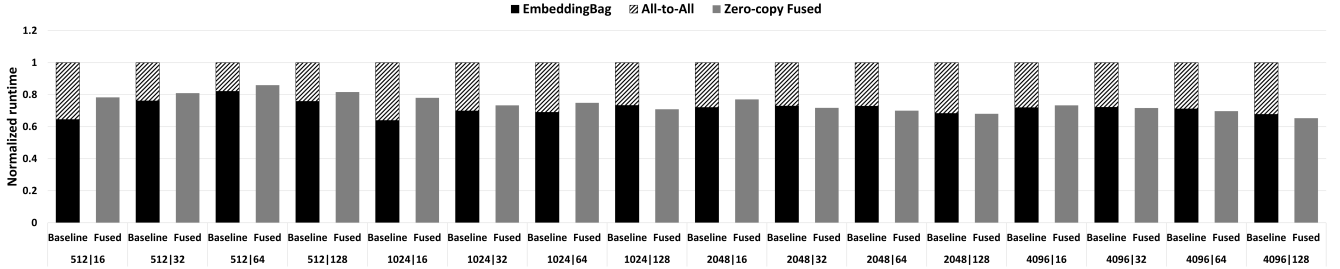


Figure 14: Normalized execution time (intra-node).

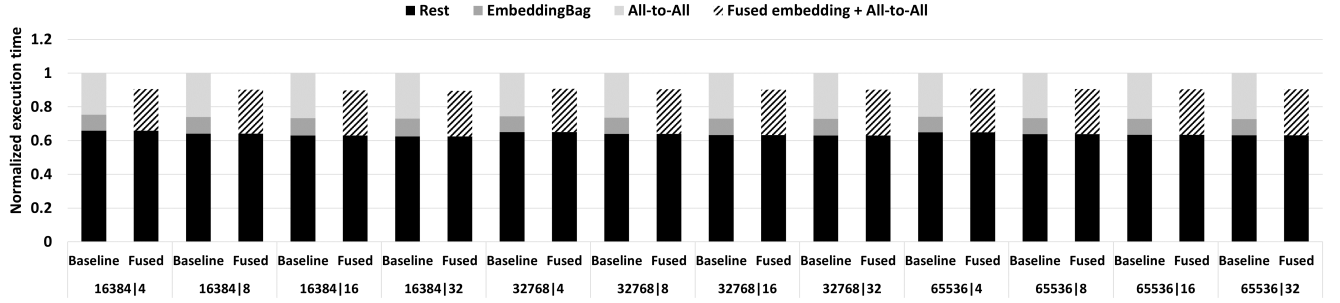


Figure 15: Scale-out execution time.

in the training and execution of current and future ML models.

In this paper, we hide the collective communication with dependent computation at a finer-granularity (cluster of WGs) using GPU-initiated communication. Our approach leverages the growing trend in HPC and ML system design where GPUs are being directly connected to CPUs, GPUs and NICs using proprietary interconnects. We exploit this tight GPU-NIC integration by triggering network transactions through GPU threads. This enables wavefront-, WG- or WG-cluster granular communication unlike CPU-initiated networking which provides kernel-granular communication. We developed fused *embedding* + *All-to-All* kernel where embedding outputs computed by a cluster of WGs are communicated in parallel to other WGs performing remainder of the computation. We propose remote communication-aware scheduling where logical WGs computing remote embedding slices are executed ahead of WGs computing local slices. This maximizes the opportunity to overlap remote communication. We further optimize the communication among P2P GPUs by developing zero-copy fused kernels. Here, GPU threads perform the embedding pooling and store the results directly to the destination address at the peer GPU, thereby eliminating intermediate stores to local memory.

We evaluated our approach both on actual hardware and using simulation. Our inter-node evaluations show that the execution time taken by fused kernel is on average 31% (and up to 58%) lower than that of baseline embedding operations and All-to-All collective. We also demonstrated the fine-grained overlapping achieved by profiling the execution of persistent WGs. We evaluated the impact of proposed communication-aware WG scheduling and show that it achieves 6% lower execution skew than communication-oblivious scheduling. Our intra-node evaluations show that zero-copy fused kernels

on average achieve 25% (and up to 35%) lower execution time than the baseline. The benefits achieved are less for intra-node evaluations than inter-node configurations due to the lower impact of intra-node All-to-All on total execution time. Finally, we used ASTRA-Sim to perform scale-out simulations to evaluate the benefits of our approach on the entire DLRM training run. Our evaluations show that using fused embedding + All-to-All kernel reduces the training time by 10% for a 128 node system.

As part of our future work, we want to use our approach to hide communication along the backward pass of DLRM. We also plan to develop fused kernels involving different collectives and computations to benefit other ML models (e.g., MoE), and parallelism strategies (e.g., fully-sharded data parallelism). Additionally, we aim to reduce the overhead incurred by using GPU-initiated communication by lowering its register and LDS usage.

REFERENCES

- [1] “AMD CDNA™ 2 ARCHITECTURE,” <https://www.amd.com/system/files/documents/amd-cdna2-white-paper.pdf>.
- [2] “AMD GCN Assembly: Cross-Lane Operations,” <https://gpuopen.com/learn/amd-gcn-assembly-cross-lane-operations/>.
- [3] “AMD Infinity Architecture,” <https://www.amd.com/en/technologies/infinity-architecture>.
- [4] ““AMD Instinct MI200” Instruction Set Architecture,” <https://www.amd.com/system/files/TechDocs/instinct-mi200-cdna2-instruction-set-architecture.pdf>.
- [5] “An Introduction to CUDA-Aware MPI,” <https://developer.nvidia.com/blog/introduction-cuda-aware-mpi/>.
- [6] “CUDAPLUGGABLEALLOCATOR,” <https://pytorch.org/docs/stable/generated/torch.cuda.CUDAPluggableAllocator.html>.

- [7] “Deep Learning Recommendation Model for Personalization and Recommendation Systems,” <https://github.com/facebookresearch/dlrm>.
- [8] “Fully Sharded Data Parallel: faster AI training with fewer GPUs,” <https://engineering.fb.com/2021/07/15/open-source/fsdp/>.
- [9] “GPUDirect RDMA,” <https://docs.nvidia.com/cuda/gpudirect-rdma/index.html#>.
- [10] “HIP: Heterogenous-computing Interface for Portability,” <https://rocm-developer-tools.github.io/HIP/>.
- [11] “IBTA Releases New InfiniBand Architecture Specification,” <https://www.infinibandta.org/ibta-releases-new-infiniband-architecture-specification/>.
- [12] “ML Parallelism,” <https://huggingface.co/docs/transformers/v4.15.0/parallelism>.
- [13] “MPI Documents,” <https://www.mpi-forum.org/docs/>.
- [14] “NCCL: Optimized primitives for inter-gpu communication,” <https://github.com/NVIDIA/nccl>.
- [15] “NVIDIA Grace Hopper Superchip Architecture In-Depth,” <https://developer.nvidia.com/blog/nvidia-grace-hopper-superchip-architecture-in-depth/>.
- [16] “NVIDIA Hopper Architecture In-Depth,” <https://developer.nvidia.com/blog/nvidia-hopper-architecture-in-depth/>.
- [17] “NVLink and NVSwitch,” <https://www.nvidia.com/en-us/data-center/nvlink/>.
- [18] “NVSHMEM,” <https://developer.nvidia.com/nvshmem>.
- [19] “OccupancyHIP API,” https://docs.amd.com/bundle/HIP-API-Guide-v5.2/page/group_occupancy.html#ga322e4690ca20dbf8a07293f2a1105c94.
- [20] “OpenSHMEM Application Programming Interface,” http://www.openshmem.org/site/sites/default/site_files/OpenSHMEM-1.5.pdf.
- [21] “ROC-profiler,” <https://github.com/ROCm-Developer-Tools/rocprowler>.
- [22] “RoCE Introduction,” <https://www.roceinitiative.org/roce-introduction/>.
- [23] “ROCm Communication Collectives Library,” <https://github.com/ROCmSoftwarePlatform/rccl>.
- [24] “ROC_SHMEM,” https://github.com/ROCm-Developer-Tools/ROC_SHMEM.
- [25] “The EPYC™ CPU and INSTINCT™ MI250X GPUs in Frontier,” <https://olcf.ornl.gov/wp-content/uploads/2-15-23-AMD-CPU-GPU-Frontier-Public.pdf>.
- [26] “TORCHSCRIPT,” <https://pytorch.org/docs/stable/jit.html>.
- [27] “XLA: Optimizing Compiler for Machine Learning,” <https://www.tensorflow.org/xla>.
- [28] M. Adnan, Y. E. Maboud, D. Mahajan, and P. J. Nair, “Accelerating recommendation system training by leveraging popular choices,” *Proc. VLDB Endow.*, 2021.
- [29] M. Boehm, B. Reinwald, D. Hutchison, P. Sen, A. V. Evfimievski, and N. Pansare, “On optimizing operator fusion plans for large-scale machine learning in systemml,” *Proc. VLDB Endow.*, 2018.
- [30] Z. Cai, Z. Liu, S. Maleki, M. Musuvathi, T. Mytkowicz, J. Nelson, and O. Saarikivi, “Synthesizing optimal collective algorithms,” in *Proceedings of the 26th ACM SIGPLAN Symposium on Principles and Practice of Parallel Programming*, 2021.
- [31] H. Fu, M. G. Venkata, A. R. Choudhury, N. Imam, and W. Yu, “High-performance key-value store on openshmem,” in *2017 17th IEEE/ACM International Symposium on Cluster, Cloud and Grid Computing (CCGRID)*, 2017.
- [32] A. Ginart, M. Naumov, D. Mudigere, J. Yang, and J. Zou, “Mixed dimension embeddings with application to memory-efficient recommendation systems,” *CoRR*, vol. abs/1909.11810, 2019. [Online]. Available: <https://arxiv.org/abs/1909.11810>
- [33] K. Gupta, J. A. Stuart, and J. D. Owens, “A study of persistent threads style gpu programming for gpgpu workloads,” in *2012 Innovative Parallel Computing (InPar)*, 2012.
- [34] U. Gupta, C.-J. Wu, X. Wang, M. Naumov, B. Reagen, D. Brooks, B. Cottel, K. Hazelwood, M. Hempstead, B. Jia, H.-H. S. Lee, A. Malevich, D. Mudigere, M. Smelyanskiy, L. Xiong, and X. Zhang, “The architectural implications of facebook’s dnn-based personalized recommendation,” in *2020 IEEE International Symposium on High Performance Computer Architecture (HPCA)*, 2020.
- [35] K. Hamidouche, A. A. Awan, A. Venkatesh, and D. K. Panda, “Cuda m3: Designing efficient cuda managed memory-aware mpi by exploiting gdr and ipc,” in *2016 IEEE 23rd International Conference on High Performance Computing (HiPC)*, 2016.
- [36] K. Hamidouche and M. LeBeane, “GPU Initiated OpenSHMEM: Correct and Efficient Intra-Kernel Networking for DGPUs,” in *Proceedings of the 25th ACM SIGPLAN Symposium on Principles and Practice of Parallel Programming*, 2020, p. 336–347.
- [37] J. Huang, P. Majumder, S. Kim, A. Muzahid, K. H. Yum, and E. J. Kim, “Communication algorithm-architecture co-design for distributed deep learning,” in *Proceedings of the 48th Annual International Symposium on Computer Architecture*, 2021.
- [38] C. Hwang, W. Cui, Y. Xiong, Z. Yang, Z. Liu, H. Hu, Z. Wang, R. Salas, J. Jose, P. Ram, J. Chau, P. Cheng, F. Yang, M. Yang, and Y. Xiong, “Tutel: Adaptive mixture-of-experts at scale,” 2022.
- [39] K. S. Khorassani, C.-H. Chu, H. Subramoni, and D. K. Panda, “Performance evaluation of mpi libraries on gpu-enabled openpower architectures: Early experiences,” in *High Performance Computing: ISC High Performance 2019 International Workshops, Frankfurt, Germany, June 16-20, 2019, Revised Selected Papers*, 2019.
- [40] S. Kim, S. Oh, and Y. Yi, “Minimizing gpu kernel launch overhead in deep learning inference on mobile gpus,” in *Proceedings of the 22nd International Workshop on Mobile Computing Systems and Applications*, 2021.
- [41] A. Li, S. L. Song, W. Liu, X. Liu, A. Kumar, and H. Corporaal, “Locality-aware cta clustering for modern gpus,” in *Proceedings of the Twenty-Second International Conference on Architectural Support for Programming Languages and Operating Systems*, 2017.
- [42] P. MacArthur and R. D. Russell, “A performance study to guide rdma programming decisions,” in *2012 IEEE 14th International Conference on High Performance Computing and Communication and 2012 IEEE 9th International Conference on Embedded Software and Systems*, 2012.
- [43] D. Mudigere, Y. Hao, J. Huang, Z. Jia, A. Tulloch, S. Sridharan, X. Liu, M. Ozdal, J. Nie, J. Park, L. Luo, J. A. Yang, L. Gao, D. Ivchenko, A. Basant, Y. Hu, J. Yang, E. K. Ardestani, X. Wang, R. Komuravelli, C.-H. Chu, S. Yilmaz, H. Li, J. Qian, Z. Feng, Y. Ma, J. Yang, E. Wen, H. Li, L. Yang, C. Sun, W. Zhao, D. Melts, K. Dhulipala, K. Kishore, T. Graf, A. Eisenman, K. K. Matam, A. Gangidi, G. J. Chen, M. Krishnan, A. Nayak, K. Nair, B. Muthiah, M. khorashadi, P. Bhattacharya, P. Lapukhov, M. Naumov, A. Mathews, L. Qiao, M. Smelyanskiy, B. Jia, and V. Rao, “Software-hardware co-design for fast and scalable training of deep learning recommendation models,” in *Proceedings of the 49th Annual International Symposium on Computer Architecture*, 2022.
- [44] M. Naumov, D. Mudigere, H. M. Shi, J. Huang, N. Sundaraman, J. Park, X. Wang, U. Gupta, C. Wu, A. G. Azzolini, D. Dzhulgakov, A. Mallevich, I. Cherniavskii, Y. Lu, R. Krishnamoorthi, A. Yu, V. Kondratenko, S. Pereira, X. Chen, W. Chen, V. Rao, B. Jia, L. Xiong, and M. Smelyanskiy, “Deep learning recommendation model for personalization and recommendation systems,” 2019.
- [45] W. Niu, J. Guan, Y. Wang, G. Agrawal, and B. Ren, “Dnnfusion: Accelerating deep neural networks execution with advanced operator fusion,” in *Proceedings of the 42nd ACM SIGPLAN International Conference on Programming Language Design and Implementation*, 2021.
- [46] S. Rajbhandari, C. Li, Z. Yao, M. Zhang, R. Y. Aminabadi, A. A. Awan, J. Rasley, and Y. He, “Deepspeed-moe: Advancing mixture-of-experts inference and training to power next-generation ai scale,” 2022.
- [47] S. Rajbhandari, J. Rasley, O. Ruwase, and Y. He, “Zero: Memory optimizations toward training trillion parameter models,” 2020.
- [48] S. Rashidi, S. Sridharan, S. Srinivasan, and T. Krishna, “ASTRA-SIM: Enabling SW/HW Co-Design Exploration for Distributed DL Training Platforms,” in *IEEE International Symposium on Performance Analysis of Systems and Software, ISPASS 2020, Boston, MA, USA, August 22-26, 2020*, 2020.
- [49] S. Rashidi, W. Won, S. Srinivasan, S. Sridharan, and T. Krishna,

- “Themis: A network bandwidth-aware collective scheduling policy for distributed training of dl models,” in *Proceedings of the 49th Annual International Symposium on Computer Architecture*, 2022.
- [50] H. M. Shi, D. Mudigere, M. Naumov, and J. Yang, “Compositional embeddings using complementary partitions for memory-efficient recommendation systems,” *CoRR*, vol. abs/1909.02107, 2019. [Online]. Available: <https://arxiv.org/abs/1909.02107>
- [51] S. Shi, X. Chu, and B. Li, “Mg-wfbp: Efficient data communication for distributed synchronous sgd algorithms,” in *IEEE INFOCOM 2019 - IEEE Conference on Computer Communications*, 2019.
- [52] P. Villalobos, J. Sevilla, T. Besiroglu, L. Heim, A. Ho, and M. Hobbhahn, “Machine learning model sizes and the parameter gap,” 2022.
- [53] S. Wang, J. Wei, A. Sabne, A. Davis, B. Ilbeyi, B. Hechtman, D. Chen, K. S. Murthy, M. Maggioni, Q. Zhang, S. Kumar, T. Guo, Y. Xu, and Z. Zhou, “Overlap communication with dependent computation via decomposition in large deep learning models,” in *Proceedings of the 28th ACM International Conference on Architectural Support for Programming Languages and Operating Systems, Volume 1*, 2022.
- [54] Y. Wang, B. Feng, Z. Wang, T. Geng, K. Barker, A. Li, and Y. Ding, “Empowering gnns with fine-grained communication-computation pipelining on multi-gpu platforms,” 2022.
- [55] M. Xie, Y. Lu, J. Lin, Q. Wang, J. Gao, K. Ren, and J. Shu, “Fleche: An efficient gpu embedding cache for personalized recommendations,” in *Proceedings of the Seventeenth European Conference on Computer Systems*, 2022.
- [56] H. Zhang, Z. Zheng, S. Xu, W. Dai, Q. Ho, X. Liang, Z. Hu, J. Wei, P. Xie, and E. P. Xing, “Poseidon: An efficient communication architecture for distributed deep learning on gpu clusters,” in *Proceedings of the 2017 USENIX Conference on Usenix Annual Technical Conference*, 2017.
- [57] M. Zhao, N. Agarwal, A. Basant, B. Gedik, S. Pan, M. Ozdal, R. Komuravelli, J. Pan, T. Bao, H. Lu, S. Narayanan, J. Langman, K. Wilfong, H. Rastogi, C.-J. Wu, C. Kozyrakis, and P. Pol, “Understanding data storage and ingestion for large-scale deep recommendation model training: Industrial product,” in *Proceedings of the 49th Annual International Symposium on Computer Architecture*, 2022.